Interactions of Na^+ Cations with a Highly Charged Fatty Acid Langmuir Monolayer: Molecular Description of the Phase Transition

Adrien Sthoer, Eric Tyrode*

Department of Chemistry, KTH Royal Institute of Technology, SE-10044 Stockholm, Sweden

* Corresponding author: tyrode@kth.se. Telephone: +46 8 7909915

Abstract

Vibrational sum frequency spectroscopy has been used to study the molecular properties upon compression of a highly charged arachidic acid Langmuir monolayer, which displays a first order phase transition plateau in the surface pressure - molecular area (π-A) isotherm. By targeting vibrational modes from the carboxylic acid headgroup, alkyl chain, and interfacial water molecules, information regarding the surface charge, surface potential, type of ion pair formed, and conformational order of the monolayer could be extracted. The monolayer in the liquid expanded phase is found to be fully charged until reaching the 2D-phase transition plateau, where partial reprotonation, as well as the formation of COO^- Na^+ contact-ion pairs, start to take place. In the condensed phase after the transition, three headgroup species, mainly hydrated COO^-, COOH, and COO^- Na^+ contact-ion pairs could be identified and their proportions quantified. Comparison with theoretical models shows that despite the low ionic strengths used (i.e. 10 mM), the predictions from the Gouy Chapman model are only adequate for the lowest surface densities, when the surface charge does not exceed -0.1 C/m^2. In contrast, a modified Poisson-Boltzmann (MPB) model that accounts for the steric effects associated with the finite ion-size, captures many of the experimental observables, including the partial reprotonation, and surface potential changes upon compression. The agreement highlights the importance of hydronium ion – carboxylate interactions, as well as the layer of sodium ions packed at the steric limit, for explaining the phase transition behavior. The MPB model, however, does not explicitly consider the formation of contact ion pairs with the sodium counterion. The experimental results provide a quantitative molecular insight that could be used to test potential extensions to the theory.

Keywords: Langmuir monolayer, arachidic acid, phase coexistence, phase transition, contact ion pair, electrical double layer, EDL, vibrational sum frequency spectroscopy, modified Poisson Boltzmann.

Introduction

The theoretical description of charged interfaces and their interaction with dissolved ions in aqueous solution have as starting point the work by Gouy and Chapman,[1-2] and the linearized Debye-Hückel[3] theory later introduce for curved surfaces. Being based on the continuum mean-field Poisson-Boltzmann (PB) theory, they rely on several simplifying assumptions,[4] including in particular, treating ions as point-like charges. These theories are typically consistent with experimental results in dilute monovalent electrolyte solutions,[4-7] but can significantly deviate at high salt concentrations, where they predict the accumulation of an unphysically large amount of counterions at the surface. The influence of the finite size of the ions was first recognized by Stern,[8] who postulated the presence of a compact layer of ions adsorbed on the surface with an adjacent diffuse double layer of the type described by Gouy and Chapman. More recent MPB models,[9-11] account for steric and excluded volume effects using a single effective ion-size parameter, that limits the concentration of counterions at the surface and smoothy describe the diffuse double layer transition. One of the implications of these MPB theories is that when subjected to large surface potentials, crowding effects can become important even in dilute solutions. Experimental confirmation of this effect remains to be tested, particularly from a molecular perspective.

Insoluble fatty acid Langmuir monolayers at the liquid/vapor interface represent useful models to study the properties of charged interfaces as they have a titratable group that can deprotonate depending on the subphase pH, ion identity and concentration, as well as temperature.[12-24] Moreover, the Langmuir trough provides direct control of the molecular surface density, giving in principle, the opportunity to vary the charge density at will. Langmuir monolayers are also amenable to characterization by several experimental techniques, including X-ray diffraction[16, 25] (unit cell and orientation of the alkyl chain in the condensed phases), X-ray reflectivity[7] (distribution of ions), Brewster angle microscopy (imaging of mesoscopic structures), and notably vibrational sum frequency spectroscopy (VSFS), which has an intrinsic surface sensitivity to detect molecules with a preferred orientation.[26]

Previous VSFS studies using arachidic acid, a fatty acid with a twenty carbon alkyl chain, have shown that the charging behavior of the monolayer at pH 6 is in excellent agreement with the Gouy Chapman model predictions for ionic strengths $\leq$ 50 mM,[23] but deviates at salt concentrations $\geq$ 100 mM.[24] For the high salt concentrations, the data was instead consistent with the steric MPB model using an effective ion size of ~7.5 Å for Na^+.[24] In those studies,

however, the charged species did not exceed 25% of the total area of the monolayer. Given that the experimentally determined apparent pKa is 10.8,[23] the pH in the subphase should go beyond this value in order to produce a highly charged surface.

The surface pressure (π)-area (A) isotherms of arachidic acid monolayers on NaOH solutions at pH of 12 or above, display, when compared to more acidic conditions, a rather complex behavior that has been the subject of numerous studies.[14, 18, 27-28] Depending on the surface density, and experimental conditions such as pH and temperature, several 2D phases can be identified, and in particular, the presence of a phase transition plateau between a liquid expanded and a condensed phase. Lacking direct molecular information about the surface species, the interpretation of the changes occurring during the transition, as well as the implications for the behavior of the charged monolayer, remain speculative at best.

In this paper, we use VSFS to investigate the molecular structural changes occurring upon compression of a highly charged arachidic acid monolayer, at a constant pH of 12 and ionic strength of 10 mM. We extract information from the charged interface by targeting selected vibrational modes. For instance, the headgroup vibrations are used to determine the surface charge and type of ion pair formed, CD stretching modes to estimate the conformational order of the alkyl chain, and OH modes from water molecules in the diffuse double layer to infer the surface potential. Moreover, information about the discreetness of the charge at the lowest surface densities is obtained from the dangling OH of water molecules straddling the surface. We show that the steric MPB model, despite its limitations, captures many of the experimental observables, including the partial reprotonation of the monolayer, observed when reaching the 2D phase transition plateau. Results highlight the importance of hydronium ion – carboxylate interactions, and their competition with sodium counterions, for describing the phase transition behavior.

Experimental Section

Materials. $NaOH.H_2O$ (99.9995%, Sigma Aldrich), eicosanoic acid (99%, AA for arachidic acid, Sigma Aldrich), perdeuterated eicosanoic acid (97%, dAA for deuterated arachidic acid, Sigma Aldrich), chloroform (anhydrous grade, stabilized with ethanol, Sigma Aldrich) were used as received. Deuterated arachidic acid is used to avoid headgroup vibrations from overlapping with CH bending and wagging modes from a perprotonated alkyl chain.[23] Salt

solutions were prepared in ultrapure water (resistivity > 18 MΩ.cm, < 3 ppb total organic content, Integral 15 Millipore system), and successively diluted to reach the desired pH value. Ethylenediaminetetraacetic acid (EDTA, 99.995% trace metal basis, Sigma Aldrich) was added to the salt solutions in concentrations ranging between 2 to 4 μM to avoid the potential adsorption of trace metal polyvalent cations to the surface, which have been shown to have a remarkable influence on the properties of the monolayers.[24, 27-28] Despite the low salt concentrations employed (i.e. 10 mM), EDTA is essential for reproducibility, because surfaces are highly charged at the pH of the experiments. Additionally, in order to remove any potential surface-active contaminants, the surface of the salt solutions was systematically aspirated several times before depositing the fatty acid monolayer. The pH of the freshly prepared solutions was within ±0.05 units of the desired value at the beginning of each experiment and remained stable within ±0.1 units during measurements.

Fatty acid monolayer and compression isotherms. Compression isotherms of the fatty acid on a NaOH subphase at different pH and temperatures were recorded on a KSV NIMA trough (150 mm wide and surface area of 77,500 mm^2), equipped with a feedback control system for adjusting and stabilizing the temperature of the subphase. Given the limited space constraints in the sample area of the spectrometer, a smaller KSV NIMA trough (50 mm wide and surface area of 9,750 mm^2) was used for the VSF spectroscopy measurements. Troughs were cleaned by wiping with a lens tissue soaked in chloroform, followed by thorough rinsing in ethanol and ultrapure water. The surface pressure was measured using a 10 mm wide paper Wilhelmy plate. After deposition of the fatty acid solution on the surface, a waiting time of at least 10 minutes was observed to ensure full solvent evaporation. The monolayers were compressed with a barrier speed of 5 $mm.min^{-1}$ when recording the full isotherms, and 10 $mm.min^{-1}$ for the spectroscopy measurements.

VSF spectrometer. The spectra have been collected with a femtosecond VSF spectrometer that has been described in detail elsewhere.[29] Briefly, the system is composed of a Ti:light oscillator (Quantronix, USA) and an Integra-HE amplifier (Amplitude, France) that generates a 1 kHz train of 90 fs pulses centered at 805 nm, with a total output power of 6 W. A large fraction of this beam (~75%) is directed to a traveling optical wave parametric amplifier (HE-TOPAS-C, Light Conversion, Lithuania) to produce the frequency tuneable broadband IR beam. The remaining fraction of the output power of the Integra is converted in a home-built beam shaper to a bandwidth tuneable picosecond pulse. The visible and tuneable IR beams were gently focused to the sample position in a co-propagating geometry, using a +1000 and

+200 mm lenses and delivered with an angle of incidence of 70°, and 55°, respectively. The generated sum frequency signal is dispersed in a spectrometer (Shamrock SR202i-B), and detected with an EM-CCD camera (Newton, Andor, Ireland). Measurements were carried out with a spectral resolution < 4 cm^{-1}. The SF signal collection optics display a high degree of automation that accommodates for changes in the angle of emission of the SF beam with IR frequency, allowing measurements in a broad spectral region (1000 cm^{-1} to 4000 cm^{-1}). The spectra were normalized by the non-resonant SF response from a gold surface following a procedure described elsewhere.[29] Unless explicitly stated, the laser powers at the sample position were set to ~4 mW (~5 mJ/cm^2) and ~40 mW (~12 mJ/cm^2) for the IR, and visible beams, respectively. When collecting SF data in the two-phase coexistent region, local temperature gradients generated by the IR beam, caused a convection flow that expelled the condensed phase from the sample position. A similar effect has been previously reported for fatty alcohols and phospholipid monolayers.[30-32] We circumvent this issue by placing an optical chopper system in the IR beam path (MC2000B with a MC1F2P10 blade with only one opening turning at 200 Hz, Thorlabs), which effectively decreases the IR power at the sample position to ~0.2 mW, and reduces the number of consecutive pulses hitting the same sample position. To decrease in signal to noise associated with this approach is compensated with longer integration times.

The spectra were fitted using a convolution of Lorentzian and Gaussian line shapes, which accounts for homogeneous and inhomogeneous broadening, as well as complex interferences between the neighboring bands.[33]

$$I_{SF} \propto \left| A_{NR}^{(2)} + \sum_{v} \int_{-\infty}^{\infty} \left(\frac{-A_v e^{-(\omega'_v - \omega_v)^2 / 2\sigma_v^2}}{\sqrt{2\pi\sigma_v^2}\left(\omega_{IR} - \omega'_v + i\Gamma_v\right)} \right) d\omega'_v \right|^2 \qquad [1]$$

A_{NR} refers to the non-resonant contribution to the SF signal, A_v to the amplitude or oscillator strength of the v^{th} resonant mode, ω_{IR}, to the infrared frequency, ω_v to the peak position, and Γ_v, and σ_v, to the Lorentzian and Gaussian line widths, respectively.

Gouy Chapman and modified Poisson Boltzmann models. The counterion profiles, surface potential, and degree of deprotonation of the fatty acid monolayer were calculated using the Gouy-Chapman theory and a modified Poisson Boltzmann model (MPB) that accounts for the finite size of the ions.[6, 10-11, 13] The acid-base equilibrium of surface bound carboxylic acid

groups, $RCOOH \rightleftharpoons RCOO^{-}+H^{+}$, relates the dissociation constant K_a, to the bulk hydronium ion concentration $[H^+]_\infty$, surface potential ψ_0, and degree of deprotonation α:

$$K_a = \frac{\alpha}{1-\alpha}\left[H^+\right]_\infty \exp^{-e\psi_0/kT} \quad [2]$$

The surface potential is in turn also dependent on the bulk ion concentration (C_∞) and surface charge, $\sigma = e\alpha/A_M$, where A_M is the area per molecule, and e the elementary charge. The surface potential for a 1:1 electrolyte is expressed as:

Gouy Chapman model: $$\psi_0 = \frac{2kT}{e}\operatorname{arcsin h}\left(\frac{\alpha e / A_M}{\sqrt{C_\infty 8\varepsilon\varepsilon_0 kT}}\right) \quad [3]$$

MPB model: $$\psi_0 = \frac{2kT}{e}\operatorname{arcsin h}\sqrt{\frac{\exp^{\left(\frac{e^2\alpha^2 a^3}{2A_M^2\varepsilon\varepsilon_0 kT}\right)}-1}{4a^3 C_\infty}} \quad [4]$$

where in the MPB model the parameter "a" represents an effective ion size.[10-11] Given that in this study the bulk hydronium ion concentration and ionic strength remain constant (pH 12), and the pK_a of the carboxylic acid is ~5.0,[23-24] the degree deprotonation as a function of area per molecule, and consequently also the surface potential, can be determined for each model by simultaneously solving equations 2 and 3, and 2 and 4.

Finally, the concentration profiles of Na^+ counterions are calculated using the following expressions:[11]

Gouy Chapman model: $$\left[Na^+\right]_x = \left[Na^+\right]_\infty \exp^{-\frac{e\psi_{(x)}}{kT}} \quad [5]$$

MPB model: $$\left[Na^+\right]_x = \frac{\left[Na^+\right]_\infty \exp^{-\frac{e\psi_{(x)}}{kT}}}{1+4a^3\left[Na^+\right]_\infty \sinh^2\left(\frac{e\psi_{(x)}}{2kT}\right)} \quad [6]$$

where the potential dependence with distance from the surface $\psi_{(x)}$ is required. For the Gouy Chapman model an analytic solution exists, but for the MPB model, $\psi_{(x)}$ is determined numerically (see supporting information for details).

Results and Discussions

1) **Compression isotherms of arachidic acid: pH and temperature dependence.**

Surface pressure vs molecular area isotherms (Π-A) of arachidic acid monolayers as a function of subphase pH and temperature are shown in Figure 1. The compression isotherm at pH 11 (Figure 1a) is essentially identical to that of pure water (pH ~5.8 in Figure 1b), where three distinct 2D phases can be observed.[16] From large areas per molecule down to ~23 $Å^2$ where the surface pressure remains constant and close to zero, we find a coexistence region between the gaseous (G) and tilted condensed (TC) phases. This is followed by the pure TC phase (also called L_2), where the alkyl chains are tilted by ~29° relatively to the surface normal,[25] and the pressure increases linearly with decreasing area. Finally, starting from the kink observed at ~27 mN/m (~19 $Å^2$ / molecule), the monolayer forms an untilted condensed (UC) phase, where the alkyl chains pack closer and are aligned parallel to the surface normal.[16, 25] Note, however, that while on pure water the monolayer is essentially fully uncharged, at pH 11 it is roughly 55% deprotonated when only the pH determining ions are present in solution.[23] The apparent insensitivity of the surface pressure isotherms to the charge of the arachidic monolayer, reflects the subtle balance between attractive (e.g., chain-chain Van der Waals interactions and hydrogen bond bridging), and repulsive forces opposing the packing, which include steric, and electrostatic interactions.[12, 14, 28]

The alkyl chains cohesive forces are eventually overcome by further deprotonating the monolayer upon increasing the pH of the subphase. This results in the expansion of the fatty acid monolayer and the appearance of additional 2D phases. In the surface pressure isotherms at pH 12 and 12.8 shown in Figure 1a, the G-TC coexistence region is replaced by a pure liquid expanded (LE) phase followed by a LE-TC coexistence region, which displays an almost constant surface pressure. The plateau region, characterized by its transition pressure ($\Pi_t > 0$) and critical area per molecule (A_t), corresponds to a first order phase transition between the LE and TC phases. Although the nature of the phase transition had long been a subject of controversy due to the non-horizontality of the plateau region, the first order has been confirmed by electron microscopy[14] and particularly BAM[28] measurements, which showed a 2D nucleation process starting from A_t with a progressive growth of domains along the plateau. The pressure of the phase transition (Π_t) can be increased by reducing the cohesive forces between the fatty acid alkyl chains, or increasing the electrostatic repulsion between the headgroups. The former effect can be achieved by increasing the temperature of the subphase

(Figure 1b), shortening the length of the alkyl chains,[28, 34-35] or adding an unsaturation,[36] while the latter is reached by further deprotonating the monolayer with increasing pH (Figure 1a).[27]

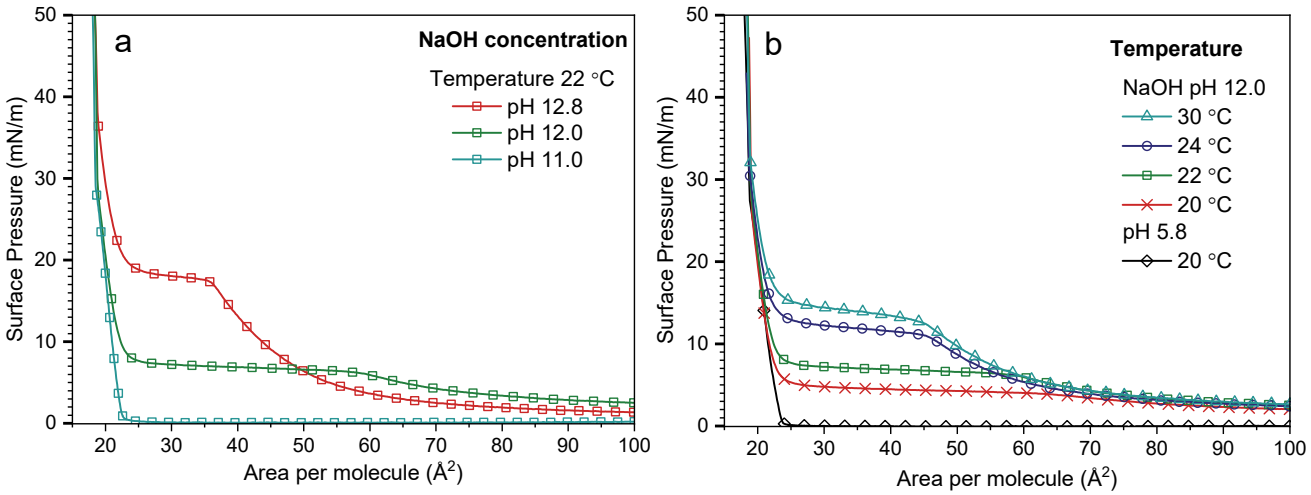

Figure 1. Compression isotherms of dAA recorded (a) at a constant temperature of 22 °C and subphase pH of 11.0, 12.0, and 12.8, and (b) at a constant pH of 12.0 at different temperatures. The isotherm on a pure water subphase is also added for reference.

Although as discussed above the fatty monolayers have structurally been extensively characterized, direct molecular information regarding the carboxylic acid headgroup along the compression isotherm at high pH is much more limited. For instance, previous attempts to theoretically determine the degree of dissociation based on the analysis of the surface pressure vs molecular area isotherms, incorrectly concluded that the monolayer is practically uncharged at pH $\leq$ 12.[27] PM-IRRAS studies showed instead that the monolayer is actually largely deprotonated at pH 12, but they do not specifically address potential changes along the phase transition.[17, 19] Recent studies using VSFS, a method more appropriate for determining the degree of ionization, have demonstrated that the monolayer is fully deprotonated at pH 13 in the liquid expanded phase (area per molecule > 40 Å^2).[23] However, it is unlikely that the monolayer stays fully dissociated upon further compression, since the surface charge density would reach values as high as -0.8 C/m^2 in the TC phase, which are significantly higher to those observed in biological membranes, where they barely exceed -0.1 C/m^2.[37] In the following sections, we use VSFS to obtain a molecular understanding of the processes occurring during the phase transition.

2) **VSF spectra of the monolayer in the pure liquid expanded and tilted condensed phases.**

Information regarding the state of dissociation and packing of the alkyl chain can be extracted from the VSF spectra. This is illustrated in the SSP polarization VSF spectrum of a dAA monolayer (~20 $Å^2$, TC phase) on pure water (pH≈5.8), which has been described in detail elsewhere,[23] and is shown here for reference in Figure 2a. The broad C-O stretch ($\nu_{C\text{-}OH}$) at ~1300 cm^{-1} and the carbonyl mode ($\nu_{C=O}$) at ~1720 cm^{-1} are associated with the uncharged carboxylic acid headgroup. From the lack of spectral features linked to the charged carboxylate moiety, expected between 1400 cm^{-1} and 1600 cm^{-1}, it is concluded that the monolayer is essentially fully protonated in pure water. On the other hand, analysis of the sharper bands centred at ~2075 cm^{-1}, ~2135 cm^{-1}, and ~2217 cm^{-1}, assigned respectively to the symmetric (r^+), Fermi resonance (r^+_{FR}), and asymmetric (r^-) stretch of the terminal CD_3 group, indicates that the deuterated alkyl chains are densely packed in an all-*trans* configuration. This scenario changes upon increasing the pH of the subphase and corresponding expansion of the monolayer.

The VSF SSP spectrum of a dAA monolayer at pH 12 and 22ºC in the pure LE phase (i.e. before the transition plateau), is shown in Figure 2b (spectra collected under the SPS and PPP polarization combinations can be found in the SI). The data is collected at a constant surface pressure of 5 mN/m, corresponding to an average molecular area of ~65 $Å^2$. In comparison to the pure water case, the bands associated with the uncharged carboxylic acid headgroup, mainly the $\nu_{C\text{-}OH}$ and $\nu_{C=O}$, are absent from the spectrum. In contrast, a new sharp band centered at ~1408 cm^{-1}, assigned to the symmetric carboxylate stretch ($\nu_{s\,COO^-}$) in a hydrated configuration (i.e. solvent-shared or solvent-separated ion pair)[15, 21-23] is observed (see Figure 2b). From the relative intensity of this band,[23] it can be deduced that the monolayer in the LE phase at 5 mN/m is fully deprotonated, corresponding to an average surface charge of -0.25 C/m^2. In the CD stretching region, compared to pure water, the spectral features are significantly weaker and linked instead to methylene modes: the symmetric (d^+) and asymmetric (d^-) CD_2 stretches centered at ~2100 cm^{-1}, and ~2200 cm^{-1}, respectively. The presence of these bands indicates that the alkyl chains are conformationally disordered with many *gauche* defects, consistent with the fluid-like character expected in the LE phase at relatively large molecular areas. Note that in spite of the disordering of the alkyl chain, the charged carboxylate headgroup remains, like an anchor, ordered and insensitive to the packing density.[23] This effect has been previously observed for other charged headgroups at the liquid/vapor interface.[38-40]

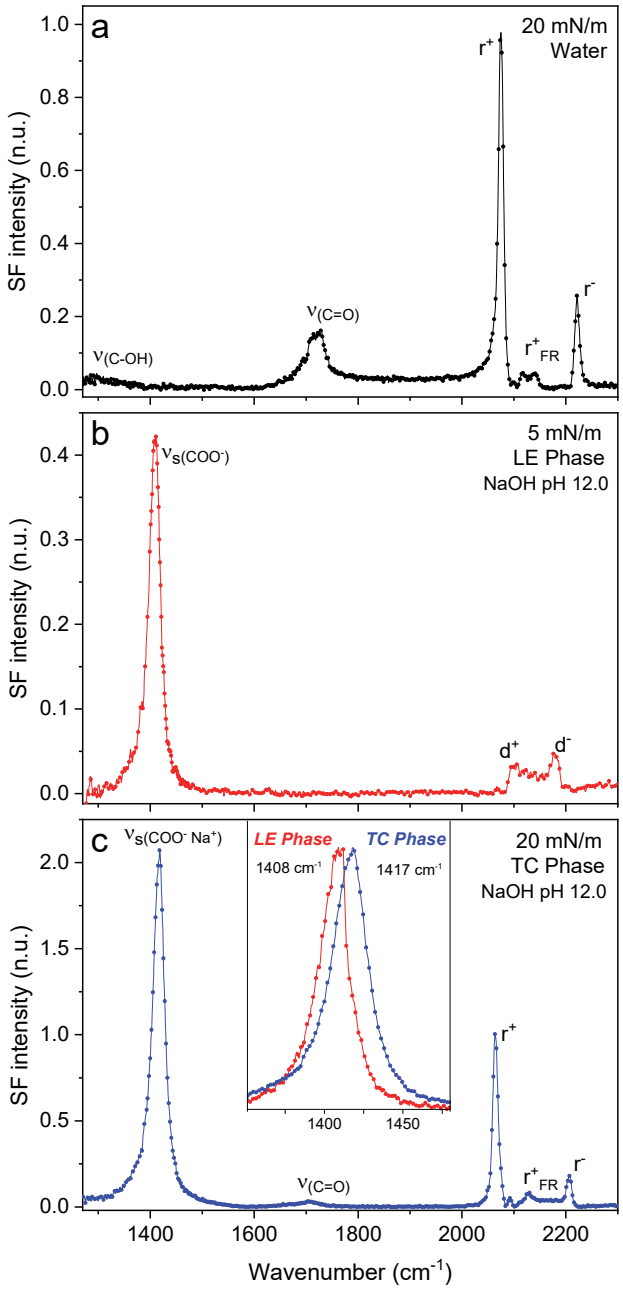

Figure 2. VSF spectra collected under the SSP polarization of a perdeuterated arachidic acid (dAA) monolayer on (a) a pure water subphase (pH ≈5.8) at a constant surface pressure of 20 mN/m (area per molecule ~20 Å^2), (b) on a NaOH subphase (pH = 12) at 5 mN/m corresponding to the pure liquid expanded (LE) phase (area per molecule ~65 Å^2), and (c) on the same pH 12 subphase but at 20 mN/m, corresponding to the pure tilted condensed (TC) phase (area per molecule ~20 Å^2). The inset in (c) highlights the blue-shift observed for the symmetric carboxylate stretch linked to the formation of a contact ion pair as a result of the phase transition (in the inset the LE spectrum intensity was multiplied by 5 to facilitate comparison). Temperature: 22°C. EDTA concentration: 4μM.

The VSF SSP spectrum for an equivalent monolayer in the pure TC phase (i.e. after the transition plateau) at a surface pressure of 20 mN/m (~20 Å^2 per molecule) is shown in Figure 2c (SPS and PPP spectra can be found in the SI). Two important differences can be identified.

First, the carbonyl stretch ($\nu_{C=O}$) at ~1720 cm^{-1}, although weaker than in the case of pure water, becomes apparent in the spectrum, indicating that the monolayer partly reprotonates after the phase transition. Second, besides an increase in intensity linked to the higher packing density, the symmetric carboxylate stretch experiences a blue shift of ~9 cm^{-1} to ~1417 cm^{-1} (see inset in Figure 2c). A similar shift has been recently reported for fatty monolayers at constant molecular areas when increasing the pH from 7 to 9 in a subphase containing 1 M LiCl,[24] and attributed, following Marcus et al. definition of ion-pairs,[41] to the formation of a contact ion pair (CIP) between Li^+ and the COO^- headgroup. Thus, the shift observed in the present case is analogously interpreted as the formation of a CIP between Na^+ and the carboxylate.

The relative proportion of fatty acid molecules that reprotonate can be estimated from the amplitude of the carbonyl stretch, having as reference the spectrum on pure water at the same packing density when the monolayer is effectively fully protonated. However, in contrast to the COO^- headgroup, the orientation of the C=O has been shown to be dependent on the degree of deprotonation of the monolayer.[24] Hence, spectra measured at two different polarization combinations, mainly SSP and SPS, are simultaneously used to estimate the proportion (see SI for details). The analysis indicates that ~33±8% of the monolayer reprotonates (i.e. $COO^- \rightarrow$ COOH) after the phase transition. Note that given the N^2 dependence of the SF intensity,[42] this corresponds to only ~10% of the $\nu_{C=O}$ intensity of a fully protonated monolayer. The direct implication is that ~2/3 of the headgroups in the monolayer remain deprotonated, but more information is required to ascertain whether all carboxylates form contact ion pairs with the sodium counterions, or if a significant fraction remains hydrated (i.e. solvent-separated or shared). This will be further discussed below when addressing the spectral changes along the phase transition. Before continuing, it is worth stressing the importance of adding EDTA to the subphase to remove trace amounts of polyvalent metallic cations, which strongly interact with the charged headgroup even when their concentration in solution does not exceed a few tens of nM.[24]

Focusing on the alkyl chain of the fatty acid, the CD stretching bands after the phase transition, are dominated by the r^+ and r^- methyl vibrations (Figure 2c). The peak intensities are approximately the same as for the pure water subphase case (see Figure 2a), confirming a similar packing density and high degree of conformational order. However, significant differences are observed in the weaker bands that appear between 2100 cm^{-1} and 2200 cm^{-1} (Figure 2c), which are mainly linked to the symmetric CD_2 stretch from the alpha-carbon next to the carboxylate headgroup, and its Fermi resonance with overtones of CD_2 deformation and

C-C skeletal stretching modes.[43-45] These overtones are known to be more sensitive to the local environment, including inductive interactions with the neighboring carboxylate headgroup.[46-48] The changes observed in the CD stretching region are thus ascribed to the formation of the contact ion pair with the sodium counterion.

3) **VSF spectral changes along the phase coexisting region.**

Examining the coexisting region between the liquid expanded and tilted condensed phases provides a deeper insight into the structural changes that occur in the monolayer. Being a first order phase transition, the relative proportion between the two phases in equilibrium is expected to vary depending on the average area per molecule. Previous BAM studies show that micrometer size domains of roughly circular shape found at the beginning of the coexisting region, grow in size to reach several tens of micrometers before forming inter-domain contacts, that eventually cover the whole surface at the end of the transition.[28] The area probed by the VSF spectrometer is ~400 x 200 μm^2 (i.e. the overlapping surface area of the IR and visible beams), thus many such domains can be probed on each laser shot (i.e. ~100 fs long), with the final spectra resulting from an average of approximately a million shots.

We first consider changes in the fatty acid alkyl chain. VSF spectra in the CD stretching region for dAA monolayers at various surface densities collected under in the SPS, SSP, and PPP polarization combinations are shown in Figure 3. The areas per molecule presented correspond to the LE phase (75 $Å^2$), the beginning of the coexisting region (60 $Å^2$), the middle of the plateau (45 $Å^2$), and the TC phase (20 $Å^2$). The SF intensity increases significantly when compressing the monolayer, reflecting not only the square dependence of the signal with the number of contributing oscillators (note that the spectra for 20 $Å^2$ denoted with a star in Figures 3a, 3b, and 3c, were divided by 4 for ease of comparison), but also its dependence on the degree of orientational order (i.e. broad angular orientational distributions results in lower signal strengths).[42, 49] Moreover, as discussed in the previous section and shown in Figure 3, at large areas per molecule (i.e. LE phase) the spectra is dominated by the methylene stretches, mostly the d^+, and d^- modes, while at higher packing densities (i.e. TC phase) it is those from the terminal methyl group that are mainly observed (i.e. r^+ and r^-). The lack of methylene SF spectral features indicate that the alkyl chains are arranged in a planar zigzag or *trans* configuration free from *gauche* defects, as the CD_2 groups become intramolecularly coupled and no longer simultaneously IR and Raman active.[42-43]

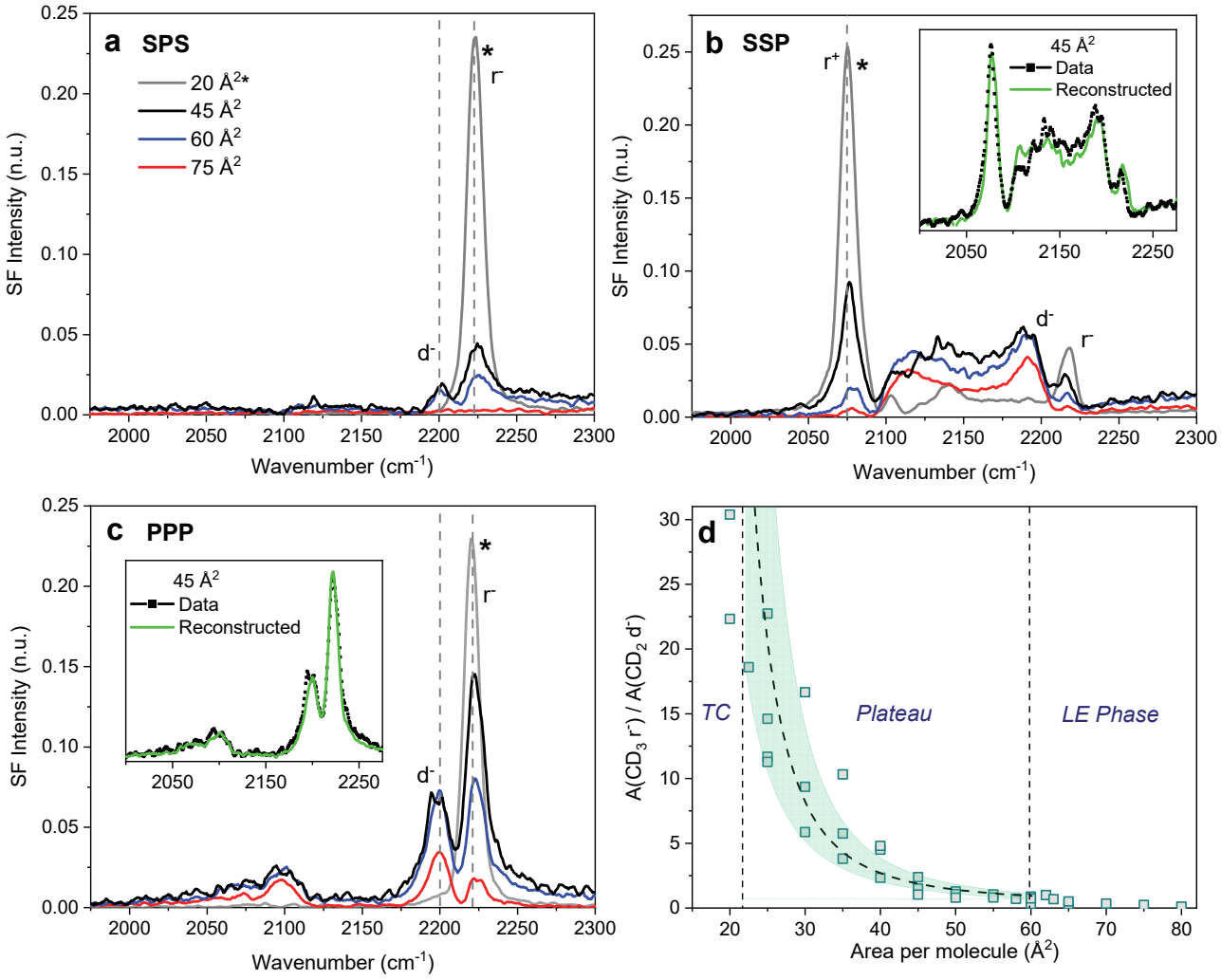

Figure 3. VSF spectra in the CD stretching region of dAA monolayers on a pH 12 NaOH subphase collected under the polarization combinations (a) SPS, (b) SSP, and (c) PPP at 4 different areas per molecule. The intensity of the 20 Å²/molecule spectra denoted with a star, were divided by 4 to facilitate comparison. Insets in (b) and (c) show 45 Å²/molecule spectra reconstructed from those of the pure phases (TC and LE) before and after the transition (green line). They closely overlap with the actual measured spectra (black squares), as expected for a first order phase transition. (d) Conformational order parameter A(CD₃ r⁻) / A(CD₂ d⁻) calculated from the fitted PPP spectra, as a function of surface density. The dashed line and green shadowed region depict the mean order parameter and corresponding error determined from reconstructed spectra at different areas per molecule (see text and SI for details). Note that spectra in the plateau region were collected using the beam chopper assembly to reduce potential heating effects (see experimental section). Temperature: 22°C. EDTA concentration:4 μM.

The conformational order of the deuterated monolayer can be tracked by following the A(CD_3 r^-) / A(CD_2 d^-) amplitude ratios in the PPP spectra, which values vary from close to zero in disordered alkyl chains, to above 15 in well-packed all-*trans* monolayers.[43] The change of this order indicator upon compression of the monolayer is summarized in Figure 3d. In the LE phase, the ratio increases from ~0.1 at 80 Å^2 to ~0.8 just before the plateau at 60 Å^2/molecule, implying a gradual ordering of the alkyl chains with higher packing densities. In the 2D phase

transition region, where domains of 60 Å^2/molecule (LE) and ~22 Å^2/molecule (TC) are found in equilibrium, the fitted r^- / d^- ratios reflect an average that depends on the relative proportion of the two phases. The insets of Figures 3b and 3c show that the spectra measured within the plateau can be accurately reconstructed from those of pure LE and TC phases just before and after the two-phase region, in accordance with the first order nature of the transition (see SI for details of the procedure). This is further visualized in the fitted A(CD_3 r^-) / A(CD_2 d^-) amplitude ratios measured during the transition, which closely matched those predicted from the reconstructed or modeled spectra at different areas per molecule (green shadowed region in Figure 3d). Finally, in the tilted condensed phase, the r^- / d^- ratio exceeds 20. The large spread in the values at high packing densities results from the d^- mode being almost absent in the PPP spectra, which induces a significant error when calculating the ratio.

We now consider changes in the fatty acid headgroup. VSF spectra of the carboxylate stretching vibrations for selected surface densities along the phase transition are shown in Figure 4a. At 60 Å^2, corresponding to the beginning of the plateau region (LE phase), the symmetric carboxylate stretch is centered at ~1408 cm^{-1} and assigned, as discussed in the previous section, to the hydrated configuration (ν_s COO^-). At the end of the transition (i.e. 20 Å^2 spectrum, TC phase), the band slightly broadens and blue shifts to ~1417 cm^{-1} due to contact ion pair formation (ν_s COO^- Na^+). Along the phase transition, the two contributing oscillators (ν_s COO^- and ν_s COO^- Na^+) are not resolved beyond shoulders in the spectra, showing instead a gradual shift in the overall peak position. Note that the lack of more distinguishable spectral features is not due to instrument limitations but to the intrinsic bandwidths of the vibrations, as no improvements were observed even when setting the spectrometer resolution < 2 cm^{-1}. Nonetheless, given that the plateau region involves two distinct phases in equilibrium, contributions from the individual bands can be readily extracted. The procedure consists in fitting the spectra in the transition region using two peaks with constrained center positions and bandwidths (see Equation 1 in experimental section). Those for the hydrated carboxylate are obtained from fits in the LE phase (areas per molecule ≥ 60 Å^2), where the ν_s COO^- is the only contributing oscillator.[23] The parameters for the ν_s COO^- Na^+ peak, are in turn obtained from fitting the spectra in the TC phase (~20 Å^2 / molecule), but with the caveat that the hydrated ν_s COO^- at 1408 cm^{-1} can still contribute to the spectral intensity (see SI for details). An example of the fit for the spectrum at 30 Å^2/molecule is shown as an inset in Figure 4a.

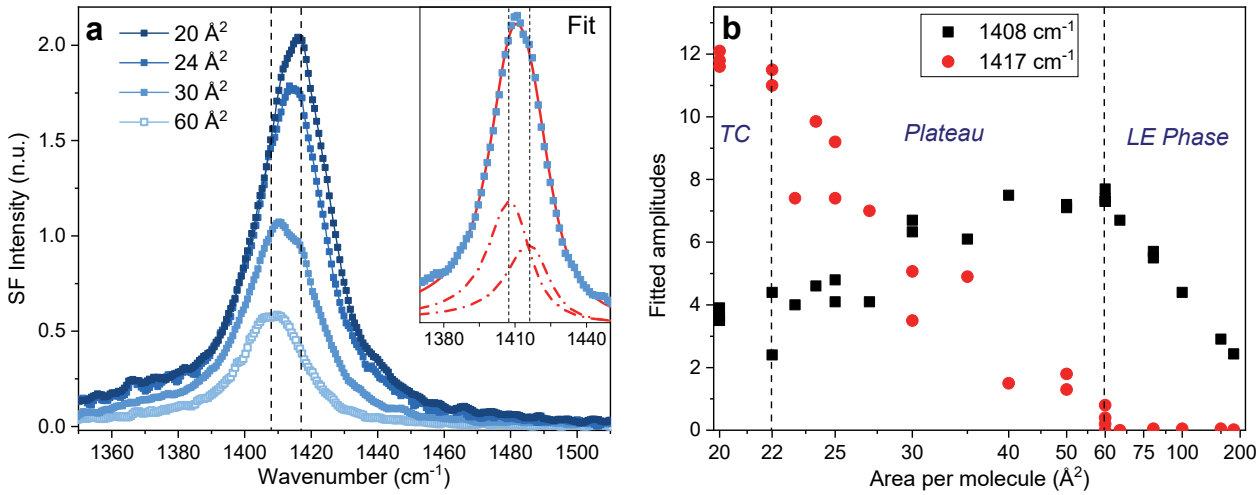

Figure 4. (a) VSF spectra in the carboxylate stretching region of dAA monolayers at different areas per molecule on a pH 12 NaOH subphase collected under the SSP polarization combination. Inset: example of a fitted spectrum (30 Å²/molecule) showing the two contributing oscillators: ν_s COO^- at ~1408 cm^{-1} and ν_s COO^- Na^+ at ~1417 cm^{-1}. (b) Fitted amplitudes for the ν_s COO^- and ν_s COO^- Na^+ peaks as a function of area per molecule. Note the reciprocal x-scale, which is linearly proportional to the molecular surface density. Spectra in the plateau region were collected using the beam chopper assembly to reduce potential heating effects (see experimental section). Temperature: 22°C. EDTA concentration: 4μM.

The fitted amplitudes as a function of area per molecule for both the ν_s COO^- and ν_s COO^- Na^+ bands are shown in Figure 4b. In the LE phase, only the hydrated carboxylate stretch is present, and its amplitude is found to be directly proportional to surface density with the data points displaying a straight line when plotted in a reciprocal scale (Figure 4b). In accordance with a previous study,[23] the implication is that the orientation of the charged headgroup, in contrast to that of the alkyl chain, remains essentially constant with packing density. However, once the plateau region is reached, the ν_s COO^- amplitude clearly departs from the linear behavior, staying approximately constant until ~40 Å^2 and decreasing thereafter to half of its value when attaining the TC phase. On the other hand, the ν_s COO^- Na^+ band (red circles in Figure 4b) shows the opposite trend, increasing from the beginning of the plateau.

The amplitude information of Figure 4b can be converted into % of monolayer coverage provided the cross-sections of the contributing bands are known. The reference for the hydrated carboxylate is readily obtained from the SF signal in the LE phase, given that only one carboxylate species is present.[23] The determination of the cross-section for ν_s COO^- Na^+ is less straightforward but can be estimated from the data in the TC phase. At 20 Å^2 /molecule three different species are found at the surface: the hydrated carboxylate (COO^-), the reprotonated carboxylic acid (COOH), and the contact ion-pair (COO^- Na^+). Since the proportions of the first two are known, the third is obtained by subtraction. The COO^- represents ~16 ± 2% of the monolayer, while COOH amounts to ~33±8% (see section 2 above). Consequently, the

proportion of $COO^- Na^+$ at 20 Å^2 is ~50±10%, implying that the cross-section for $\nu_{s\,COO^- Na^+}$ is within ± 15% equivalent to that of $\nu_{s\,COO^-}$.

Figure 5 depicts the fraction of each species as a function of area per molecule plotted in a reciprocal scale, where the percentage of uncharged carboxylic moieties in the two-phase region is determined by subtraction. In the plateau region, the relative amount of hydrated carboxylate species decrease at the expense of forming contact ion pairs with sodium, and the condensation of hydronium counterions.

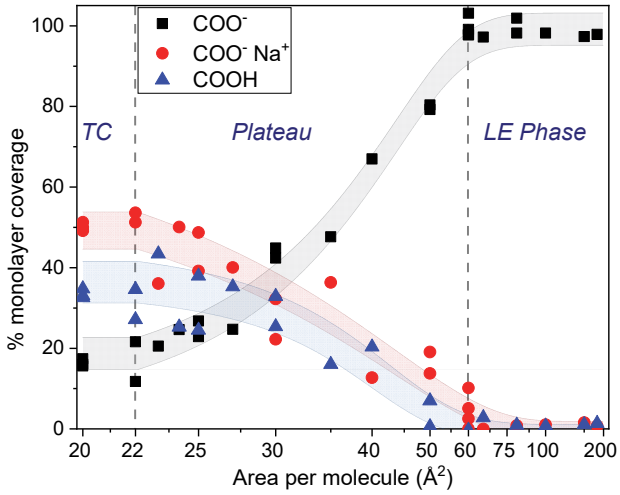

Figure 5. Estimated percentage of monolayer coverage of hydrated carboxylate (COO^-), contact ion pair (COO^-Na^+), and uncharged carboxylic acid (COOH) species as a function of surface density. Note the reciprocal x-scale, which is linearly proportional to the molecular surface density. The proportion of COOH was determined by subtraction (see text). The gray, red, and blue shaded regions are added as guides to the eye. Monolayer: dAA on a pH 12 NaOH subphase. Temperature: 22°C. EDTA concentration: 4μM.

4) **Water response in the diffuse double layer: surface potential and comparison with theoretical models.**

Additional information of the charged monolayer can be extracted from the response of water molecules in the immediate surface and in particular, those in the diffuse double layer interacting with the surface electric field. The SF spectra in the CH and OH stretching regions of a per-protonated arachidic acid monolayer for selected areas per molecule are shown in Figure 6a. In the CH stretching region the spectra show four distinct contributions at ~2845 cm^{-1}, ~2875 cm^{-1}, ~2940 cm^{-1} and a shoulder at ~2960 cm^{-1}, corresponding to the methylene (d^+) and methyl (r^+) symmetric stretches, the Fermi resonance (r^+_{FR}) of the terminal methyl, and its

asymmetric stretch (r^-), respectively.[43, 50-51] Upon compression, the vibrational signatures from the terminal CH_3 group dominate over those from the methylenes. This is in accordance with the interpretation made for the per-deuterated analog, where the conformational order increases with the packing of the monolayer.

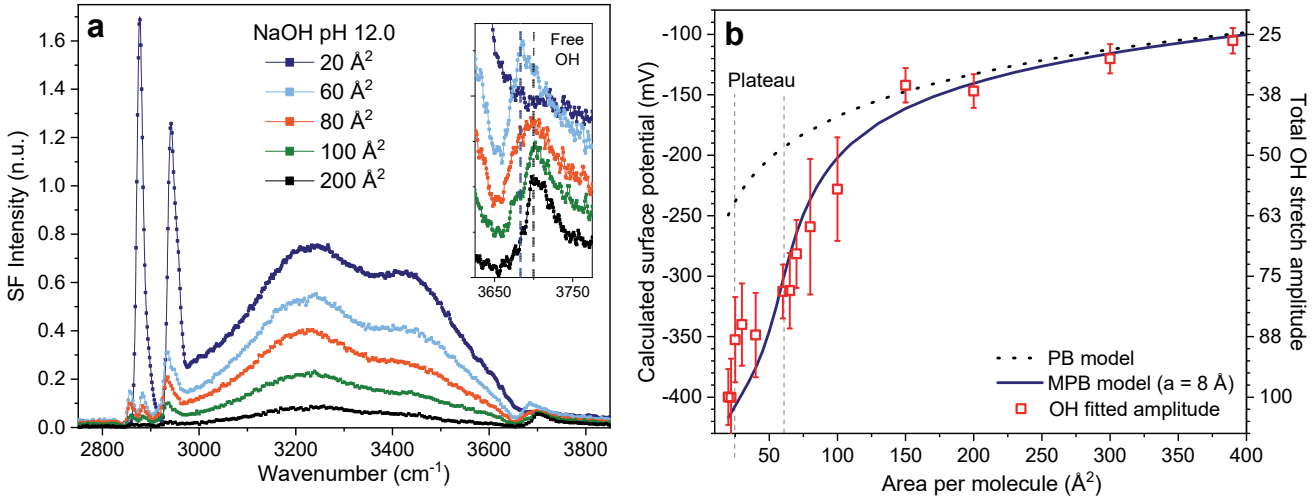

Figure 6. (a) VSF spectra in the CH and OH stretching regions of AA monolayers at different areas per molecule on a pH 12 NaOH subphase collected under the SSP polarization combination. Inset: expanded view of the dangling OH stretching region (spectra were offset 0.01 units for ease of comparison), where two peaks can be identified. (b) Surface potential as a function of area per molecule calculated using the Gouy Chapman theory (PB) and a modified Poisson-Boltzmann model (MPB) that accounts for steric effects (a=8 Å). Right axis: fitted OH amplitudes as a function of area per molecule (red open squares). Error bars represent one standard deviation of the mean obtained from replicate measurements. Note that the scales are linearly proportional to each other. Spectra in the plateau region were collected using the beam chopper assembly to reduce potential heating effects (see experimental section). Temperature: 22°C. EDTA concentration: 4μM.

Significant changes can also be observed in the OH stretching region upon compression of the monolayer. Focusing first on the dangling OH response (>3650 cm^{-1}), a single peak centered at ~3700 cm^{-1} is resolved in the spectra (see inset in Figure 6a) at large molecular areas (i.e., ≥ 200 $Å^2$ / molecule). However, when increasing the packing density in the liquid expanded phase, a new band centered at ~3680 cm^{-1} is seen to appear. First observed as a shoulder (i.e., 100 $Å^2$ / molecule), the peak gains in intensity, eventually becoming the dominant, if not only contributor, when reaching the phase transition at 60 $Å^2$ / molecule. Finally, at the higher packing densities of the tilted condensed phase, dangling OHs are no longer observed (see inset in Figure 6a). These changes can be interpreted as follows. For the lower surface densities, the fatty acid molecules cover only a small fraction of the surface, leaving large areas where water molecules directly interact with the gas phase. The peak at ~3700 cm^{-1} is consistent with the assignment of a dangling OH vibrating in air free from hydrogen bonds.[52] With the

compression of the monolayer, the proportion of bare patches decreases, and interactions between water and the alkyl chain of arachidic acid molecules become more dominant. Due to the free energy gain of reducing air/water contacts,[53] the majority of the hydrocarbon chains, which in the liquid expanded phase display a large proportion of *gauche* defects, reside in the plane of the surface. Water molecules in contact with these chains also exhibit a dangling OH, but ~20 cm^{-1} red-shifted when compared to air,[54-55] explaining the appearance of the ~3680 cm^{-1} band shown in the inset of Figure 6a. Lastly, for the highest packing densities, where the alkyl chains are upright and conformationally ordered in an all *trans* configuration, water molecules only interact through hydrogen bonds with the polar or charged carboxylic acid headgroup, leading to the absence of dangling OH features in the spectra.

When considering the bonded OH stretching region that extends between ~3000 cm^{-1} and ~3600 cm^{-1}, the SF intensity increases significantly with packing density (Figure 6a), with the spectral shape remaining almost invariant. The band contains contributions from water molecules directly interacting with the carboxylic acid headgroups (i.e. $\chi^{(2)}$), as well as those further into the bulk in the diffuse double layer (i.e. $\chi^{(3)}$). However, the former are negligible given the relatively low ionic strengths (i.e. 10 mM) and high surface charge densities experience at pH 12. The signal from these molecules in the immediate surface becomes only apparent at higher salt concentrations or in pure water, when the diffuse layer response is either substantially screened or mostly canceled by destructive interference as shown elsewhere.[23-24] With an ionic strength of 10 mM, the Debye length is significantly shorter than the non-linear coherence length, and the signal from water molecules in the probed double layer region does not experience interference and add only constructively.[56-57] The amplitudes of the bonded OH bands are then expected to be directly proportional to the surface potential.[58]

The fitted amplitudes of the bonded OH modes as a function of area per molecule are summarized in Figure 6b. The experimental results are compared with the surface potentials calculated using the Gouy-Chapman theory (PB), and a modified Poisson Boltzmann (MPB) model that accounts for the finite size of the counterions, using a = 8 Å as effective ion-size (see experimental section).[10-11] This value is in the range of those reported for the hydrated Na^+ cation diameter (~7.2 – 8.0 Å),[59-62] as well as that estimated in a previous VSF study performed at a lower pH but much higher ionic strengths.[24] In contrast to the MPB predictions, the PB model fails to reproduce the experimental trends for the highest packing densities, highlighting the importance of steric effects at highly charged surfaces.[11] The PB model, treating ions as

point charges, underestimates the surface potential because it allows the accumulation of counterions to unphysically high concentrations. This is illustrated in the Na^+ density profiles shown in Figure 7a, calculated using the PB and MPB model for selected areas per molecule (see the experimental section for calculation details). At surface densities ≥200 $Å^2$/molecule both models predict similar profiles. However, when the surface charge exceeds -0.1 C/m^2, the differences become apparent. For instance, at 100 $Å^2$/molecule the PB model predicts a surface concentration of sodium ions that already exceeds the solubility limit of NaCl in the bulk (~6 M), and at 20 $Å^2$/molecule the calculated value is well in excess of 150 M!. On the other hand, the MPB model limits the maximum concentration of counterions at the surface, inducing the formation of a saturated layer of hydrated cations at the highest charge densities (see Figure 7a),[10-11] and consequently, larger surface potentials due to the reduced screening (Figure 6b).

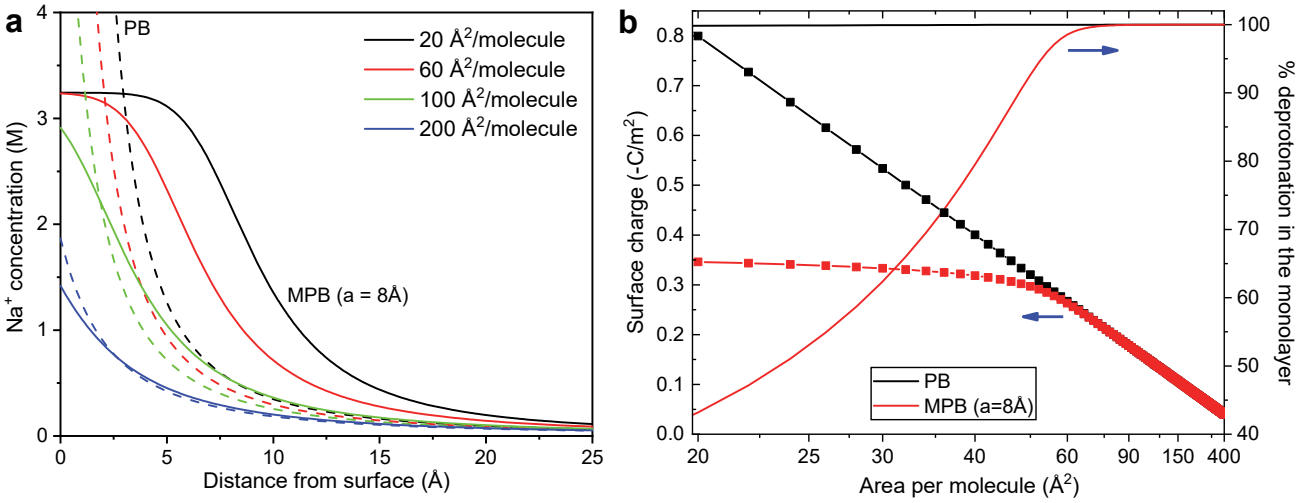

Figure 7. (a) Surface density profile of Na^+ counterions for selected areas per arachidic acid molecule, calculated using the Gouy Chapman theory (dashed lines) and the steric MPB model (solid lines, a=8 Å). (b) Surface charge (squared symbols, left axis), and monolayer percentage of deprotonation (solid lines, right axis) as a function of area per molecule, calculated using the Gouy Chapman theory (PB- in black) and the MPB model (in red).

As depicted in Figure 7b, the MPB model also predicts, in qualitative agreement with experimental results, the partial reprotonation of the monolayer upon compression. This is in contrast to the PB model, which predicts that the monolayer remains almost fully deprotonated even at 20 $Å^2$/molecule (Figure 7b). The departure between the two models occurs at approximately 60 $Å^2$/molecule, which closely coincides with the critical area of the phase transition (Figure 1). Note that the calculated critical density will depend on the effective ion size chosen.

5) **Molecular description of the charged monolayer: final discussion.**

The combination of all experimental results provides a valuable molecular insight into the structural changes occurring in the interfacial region as a function of charge density. From the analysis of the center frequency and amplitude of the symmetric carboxylate stretch, it is concluded that the monolayer in the liquid expanded phase is fully charged and the headgroup is exclusively found in a hydrated configuration (i.e. no formation of contact-ion pairs). Consequently, the surface charge in the LE phase increases linearly with the surface density up to 60 $Å^2$/molecule (see Figure 4b), an observation that is consistent with both the PB and MPB model predictions (Figure 7b). However, the response from water in the diffuse double layer indicates that the surface potential decreases more rapidly (i.e. becomes more negative) than what the Gouy Chapman theory suggests, but well in accordance with the MPB model when setting the effective ion size to ~8Å. Steric effects that limit the concentration of sodium counterions at the surface, become then experimentally apparent for areas per molecule lower than 150 $Å^2$ when the surface charge exceeds approximately -0.1 C/m^2. We note that for a lower pH but higher ionic strengths (i.e., pH 6, NaCl >50 mM) a similar critical charge needs to be reached before the finite size of the sodium cations has an influence.[24] Another interesting aspect that draws attention to the discreteness of the surface charge, is the dangling OH signal from water molecules straddling the surface (Figure 6a), which presences shows that for the lowest surface densities, fatty acid molecules are sufficiently far apart from each other to leave patches of pure water in direct contact with air. These bare patches are substituted at the end of the LE phase for water – oil contacts, formed with the configurationally disordered hydrocarbon alkyl chains that lay mostly on the plane of the surface.

Once the 2D phase transition region is reached, the surface charge no longer increases linearly with monolayer density, as not only contact ion pairs between COO^- and Na^+, but also reprotonated COOH groups, start forming in a close to equal proportions (Figure 5). Given that the concentration of H^+ in the bulk is 10 orders of magnitude lower than Na^+ (i.e. 1 pM compared to 10 mM), the similar proportions between the two species (COOH / COO^- Na^+), emphasizes the considerably higher affinity of hydronium ions for the charged carboxylate moiety. It also hints on the potential influence of the counterion's identity in the behavior of the phase transition, as Li^+ and Cs^+ ions have been shown to have, relative to Na^+, higher, and lower affinities, respectively, to the charged carboxylate.[24]

The amplitude of the hydrated ν_s COO^- mode, decreases at the end of the phase transition by approximately 50% when compared to the starting value at 60 $Å^2$ / molecule (Figure 4b). If the hydrated carboxylate was the only species responsible for the surface charge, the latter will be expected to decrease accordingly. However, the experimental data from the OH stretching region, which is directly linked to the surface potential, conclusively show that the surface charge continues to increase, albeit at a lower rate, during and after the plateau (Figure 6b). The implication is that the COO^- Na^+ contact ion pairs contribute, at least partially, to the total surface charge. It is estimated that the contribution per contact ion pair is equivalent to roughly 50% of the elementary charge.

In contrast to the charged carboxylate headgroup, which orientation was found to be largely independent of the surface density, the conformational order of the alkyl chain varied significantly with compression. From being conformationally disordered and laying close to the surface plane with a large number of *gauche* defects at the largest area per molecule examined, to conformationally ordered all-*trans* monolayers in the TC phase. In the LC/TC transition region, the measured spectra could be readily reconstructed from that of the pure phases before and after the transition, providing additional support for the phase transition being of first order.

When comparing the results with theory, it is evident that the modified PB model that accounts for the finite size of the ions,[10-11] captures many of the experimental observables. The formation of a saturated layer of sodium counterions packed at the steric limit next to the surface, explains the rapid increase, in absolute terms, of the surface potential (Figure 6b). The increased potential eventually leads to the partial reprotonation of the monolayer due to the substantial boost in the amount of hydronium ion at the surface (Figure 7b). Moreover, the predicted surface density at which reprotonation starts to take place coincides with the commencement of the 2D phase transition region in the surface pressure isotherms. It is worth noting that the model also predicts a correct behaviour when increasing the pH of the subphase or ionic strength at constant pH, letting the monolayer attain higher charge densities before reaching the phase transition (see SI). The MPB model used offers the advantage of describing the potential drop from the surface in a continuous fashion, without the discontinuities associated with layer models that separate an inner "condensed" region of ions from those in the diffuse double layer, as is the case for the Stern phenomenological model.[8] Having said this, the MPB model does not explicitly account for the formation of contact ion pairs between Na^+ and COO^-, as the predicted partial reprotonation results exclusively from the condensation of hydronium

ions upon compression of the monolayer. Additionally, if not through the effective ion-size, that acts as a phenomenological fitting parameter, the MPB model does not consider the potential influence of other relevant physical phenomena,[63] such as the non-uniform dielectric response close to the surface,[64] dispersion interactions,[65-66] ion-ion correlations,[67-68] or solvent effects.[69]

Conclusions

VSF spectroscopy, combined with the Langmuir trough technique, has provided detailed and quantitative molecular information of the changes occurring upon compression of a highly charged insoluble fatty acid monolayer. At a temperature of 22 ºC and constant subphase pH of 12, the monolayer is found to be fully charged in the liquid expanded phase, which corresponds to areas per molecules larger than ~60 $Å^2$, or a surface charge ≥ ~-0.26 C/m^2. Upon further compression, the monolayer is characterized by a first order phase transition between the LE and tilted condensed phases,[27] which triggers the partial reprotonation of the monolayer by condensation of hydronium ions on the carboxylate headgroup, as well as the formation of $COO^- Na^+$ contact ion pairs. At the end of the transition in the pure TC phase, the three headgroup species identified consist of COOH, $COO^- Na^+$, and hydrated COO^-, found roughly in a 2:3:1 proportion. Additionally, from the analysis of the spectroscopic response of water molecules in the diffuse double layer, it was concluded that the surface potential, and consequently, the surface charge, continues to rise when compressing the monolayer in the 2D phase region up to ~-0.34 C/m^2. The implication is that $COO^- Na^+$ contact ion pairs must partially contribute to the charge of the monolayer.

When compared with theoretical models, the experimental results are only consistent with the Gouy Chapman predictions at low charge densities (surface charge > ~-0.1 C/m^2). At higher surface charges, the experimental data is in good agreement with an MPB model that accounts for the finite size of the counterion.[10-11] The MPB model predicts the correct surface potential dependence, the partial reprotonation of the monolayer due to hydronium ion condensation, as well as its pH dependence. However, it does not consider the formation of $COO^- Na^+$ contact ion pairs, nor the potential influence of other relevant interactions. The experimental results presented here could be used as a benchmark for testing the suitability of extended theories that simultaneously account for physical phenomena not explicitly included in the MPB model description.[18, 70]

Acknowledgments

Funding by the Swedish Research Council (VR) and the Swedish Foundation for Strategic Research (SSF) through the program "Future Research Leaders-5", are gratefully acknowledged.

Supporting Information Available:

Expresions for the potential dependence with distance based on the Gouy Chapman and steric-MPB models, VSF spectra in the SPS and PPP polarization combination, fitting procedures for determinining the percentage of reprotonation, hydrated carboxylate / contact ion pair ratio, and surface potential, spectra reconstruction in the phase transition region, and steric-MPB predictions at higher pH and temperatures.

References

1. Gouy, G., Sur La Constitution De La Charge Électrique À La Surface D'un Électrolyte. *C. R. Seances Acad. Sci.* **1909**, *149*, 654-657.
2. Chapman, D. L., Li. A Contribution to the Theory of Electrocapillarity. *Lond. Edinb. Dubl. Phil. Mag.* **1913**, *25*, 475-481.
3. Debye, P.; Hückel, E., Zur Theorie Der Elektrolyte. I. Gefrierpunktserniedrigung Und Verwandte Erscheinungen. *Physikalische Zeitschrift* **1923**, *24*, 185-206.
4. Evans, D. F.; Wennerström, H., *The Colloidal Domain: Where Physics, Chemistry, Biology, and Technology Meet, 2nd*, 1998, p 640 pp.
5. Verwey, E. J. N.; Overbeek, J. T. G., *Theory of Stability of Lyophobic Colloids*; Elsevier: Amsterdam, 1948.
6. Israelachvili, J. N., *Intermolecular and Surface Forces* Third ed.; Elsevier: Oxford, 2011, p 674.
7. Bu, W.; Vaknin, D.; Travesset, A., How Accurate Is Poisson−Boltzmann Theory for Monovalent Ions near Highly Charged Interfaces? *Langmuir* **2006**, *22*, 5673-5681.
8. Stern, O., Zur Theorie Der Elektrolytischen Doppelschicht. *Z. Elektrochem. Angew. Phys. Chem.* **1924**, *30*, 508-516.
9. Kralj-Iglič, V.; Iglič, A., A Simple Statistical Mechanical Approach to the Free Energy of the Electric Double Layer Including the Excluded Volume Effect. *Journal de Physique II* **1996**, *6*, 477-491.
10. Borukhov, I.; Andelman, D.; Orland, H., Steric Effects in Electrolytes: A Modified Poisson-Boltzmann Equation. *Phys. Rev. Lett.* **1997**, *79*, 435-438.
11. Kilic, M. S.; Bazant, M. Z.; Ajdari, A., Steric Effects in the Dynamics of Electrolytes at Large Applied Voltages. I. Double-Layer Charging. *Phys. Rev. E* **2007**, *75*, 021502.
12. Gaines, G. L., *Insoluble Monolayers at Liquid-Gas Interfaces*; Wiley (Interscience): New York, 1966, p 383.
13. Pezron, E.; Claesson, P. M.; Berg, J. M.; Vollhardt, D., Stability of Arachidic Acid Monolayers on Aqueous Salt Solutions. *Journal of Colloid and Interface Science* **1990**, *138*, 245-254.

14. Oishi, Y.; Takashima, Y.; Suehiro, K.; Kajiyama, T., Effect of Ionic Repulsion among Hydrophilic Groups on Aggregation Structure of Fatty Acid Monolayer on the Water Surface. *Langmuir* **1997**, *13*, 2527-2532.
15. Miranda, P. B.; Du, Q.; Shen, Y. R., Interaction of Water with a Fatty Acid Langmuir Film. *Chem. Phys. Lett.* **1998**, *286*, 1-8.
16. Kaganer, V. M.; Möhwald, H.; Dutta, P., Structure and Phase Transitions in Langmuir Monolayers. *Rev. Mod. Phys.* **1999**, *71*, 779-819.
17. Le Calvez, E.; Blaudez, D.; Buffeteau, T.; Desbat, B., Effect of Cations on the Dissociation of Arachidic Acid Monolayers on Water Studied by Polarization-Modulated Infrared Reflection−Absorption Spectroscopy. *Langmuir* **2001**, *17*, 670-674.
18. Johann, R.; Vollhardt, D.; Möhwald, H., Shifting of Fatty Acid Monolayer Phases Due to Ionization of the Headgroups. *Langmuir* **2001**, *17*, 4569-4580.
19. Johann, R.; Vollhardt, D.; Möhwald, H., Study of the Ph Dependence of Head Group Bonding in Arachidic Acid Monolayers by Polarization Modulation Infrared Reflection Absorption Spectroscopy. *Colloids Surf., A* **2001**, *182*, 311-320.
20. Ye, S.; Noda, H.; Nishida, T.; Morita, S.; Osawa, M., Cd2+-Induced Interfacial Structural Changes of Langmuir−Blodgett Films of Stearic Acid on Solid Substrates: A Sum Frequency Generation Study. *Langmuir* **2004**, *20*, 357-365.
21. Tang, C. Y.; Allen, H. C., Ionic Binding of Na+ Versus K+ to the Carboxylic Acid Headgroup of Palmitic Acid Monolayers Studied by Vibrational Sum Frequency Generation Spectroscopy. *J. Phys. Chem. A* **2009**, *113*, 7383-7393.
22. Tang, C. Y.; Huang, Z.; Allen, H. C., Binding of Mg2+ and Ca2+ to Palmitic Acid and Deprotonation of the Cooh Headgroup Studied by Vibrational Sum Frequency Generation Spectroscopy. *J. Phys. Chem. B* **2010**, *114*, 17068-17076.
23. Tyrode, E.; Corkery, R., Charging of Carboxylic Acid Monolayers with Monovalent Ions at Low Ionic Strengths: Molecular Insight Revealed by Vibrational Sum Frequency Spectroscopy. *J. Phys. Chem. C* **2018**, *122*, 28775-28786.
24. Sthoer, A.; Hladilkova, J.; Lund, M.; Tyrode, E., Molecular Insight into Carboxylic Acid - Alkali Metal Cations Interactions: Reversed Affinities and Ion-Pair Formation Revealed by Non-Linear Optics and Simulations. *Phys. Chem. Chem. Phys* **2019**, *21*, 11329-11344.
25. Kenn, R. M.; Boehm, C.; Bibo, A. M.; Peterson, I. R.; Möhwald, H.; Als-Nielsen, J.; Kjaer, K., Mesophases and Crystalline Phases in Fatty Acid Monolayers. *J. Phys. Chem.* **1991**, *95*, 2092-2097.
26. Shen, Y. R.; Ostroverkhov, V., Sum-Frequency Vibrational Spectroscopy on Water Interfaces: Polar Orientation of Water Molecules at Interfaces. *Chem. Rev.* **2006**, *106*, 1140-1154.
27. Fainerman, V. B.; Vollhardt, D.; Johann, R., Arachidic Acid Monolayers at High Ph of the Aqueous Subphase: Studies of Counterion Bonding. *Langmuir* **2000**, *16*, 7731-7736.
28. Johann, R.; Vollhardt, D., Texture Features of Long-Chain Fatty Acid Monolayers at High Ph of the Aqueous Subphase. *Mater. Sci. Eng.* **1999**, *8*, 35-42.
29. Liljeblad, J. F. D.; Tyrode, E., Vibrational Sum Frequency Spectroscopy Studies at Solid/Liquid Interfaces: Influence of the Experimental Geometry in the Spectral Shape and Enhancement. *J. Phys. Chem. C* **2012**, *116*, 22893-22903.
30. Casson, B. D.; Braun, R.; Bain, C. D., Phase Transitions in Monolayers of Medium-Chain Alcohols on Water Studied by Sum-Frequency Spectroscopy and Ellipsometry. *Faraday Discuss.* **1996**, *104*, 209-229.
31. Backus, E. H. G.; Bonn, D.; Cantin, S.; Roke, S.; Bonn, M., Laser-Heating-Induced Displacement of Surfactants on the Water Surface. *J. Phys. Chem. B* **2012**, *116*, 2703-2712.
32. Franz J., V. Z. M. J., Weidner T., A Trough for Improved Sfg Spectroscopy of Lipid Monolayers. *Review of Scientific Instruments* **2017**, *88*, 053106.

33. Bain, C. D.; Davies, P. B.; Ong, T. H.; Ward, R. N.; Brown, M. A., Quantitative Analysis of Monolayer Composition by Sum-Frequency Vibrational Spectroscopy. *Langmuir* **1991**, *7*, 1563-6.
34. Goddard, E. D.; Kao, O.; Kung, H. C., Monolayer Properties of Fatty Acids: Iv. Influence of Cation at High Ph. *J. Colloid Interface Sci.* **1967**, *24*, 297-309.
35. Rivière, S.; Hénon, S.; Meunier, J.; Schwartz, D. K.; Tsao, M. W.; Knobler, C. M., Textures and Phase Transitions in Langmuir Monolayers of Fatty Acids. A Comparative Brewster Angle Microscope and Polarized Fluorescence Microscope Study. *J. Chem. Phys.* **1994**, *101*, 10045-10051.
36. Tyrode, E.; Niga, P.; Johnson, M.; Rutland, M. W., Molecular Structure Upon Compression and Stability toward Oxidation of Langmuir Films of Unsaturated Fatty Acids: A Vibrational Sum Frequency Spectroscopy Study. *Langmuir* **2010**, *26*, 14024-14031.
37. Pekker, M.; Shneider, M., Interaction between Electrolyte Ions and the Surface of a Cell Lipid Membrane. *J Phys Chem Biophys* **2015**, *5*, 177.
38. Tyrode, E.; Johnson, C. M.; Rutland, M. W.; Day, J. P. R.; Bain, C. D., A Study of the Adsorption of Ammonium Perfluorononanoate at the Air-Liquid Interface by Vibrational Sum-Frequency Spectroscopy. *J. Phys. Chem. C* **2007**, *111*, 316-329.
39. Zdrali, E.; Chen, Y.; Okur, H. I.; Wilkins, D. M.; Roke, S., The Molecular Mechanism of Nanodroplet Stability. *ACS Nano* **2017**, *11*, 12111-12120.
40. Johnson, C. M.; Tyrode, E., Study of the Adsorption of Sodium Dodecyl Sulfate (Sds) at the Air/Water Interface: Targeting the Sulfate Headgroup Using Vibrational Sum Frequency Spectroscopy. *Phys. Chem. Chem. Phys* **2005**, *7*, 2635-2640.
41. Marcus, Y.; Hefter, G., Ion Pairing. *Chem. Rev.* **2006**, *106*, 4585-4621.
42. Bain, C. D., Sum-Frequency Vibrational Spectroscopy of the Solid/Liquid Interface. *J. Chem. Soc., Faraday Trans.* **1995**, *91*, 1281-96.
43. Tyrode, E.; Hedberg, J., A Comparative Study of the Cd and Ch Stretching Spectral Regions of Typical Surfactants Systems Using Vsfs: Orientation Analysis of the Terminal Ch3 and Cd3 Groups. *J. Phys. Chem. C* **2012**, *116*, 1080-1091.
44. MacPhail, R. A.; Strauss, H. L.; Snyder, R. G.; Elliger, C. A., Carbon-Hydrogen Stretching Modes and the Structure of N-Alkyl Chains. 2. Long, All-Trans Chains. *J. Phys. Chem.* **1984**, *88*, 334-41.
45. Sunder, S.; Mendelsohn, R.; Bernstein, H. J., Raman Studies of the C-H and C-D Stretching Regions in Stearic Acid and Some Specifically Deuterated Derivatives. *Chemistry and Physics of Lipids* **1976**, *17*, 456.
46. Henry, B. R.; Miller, R. J. D., Intramolecular Perturbation of Ch-Stretching Diagonal Local Mode Anharmonicity in Methyl Substituted Alkanes. *Chemical Physics Letters* **1978**, *60*, 81-84.
47. Zhang, D.; Gutow, J.; Eisenthal, K. B., Vibrational Spectra, Orientations, and Phase Transitions in Long-Chain Amphiphiles at the Air/Water Interface: Probing the Head and Tail Groups by Sum Frequency Generation. *The Journal of Physical Chemistry* **1994**, *98*, 13729-13734.
48. Hsi, S. C.; Tulloch, A. P.; Mantsch, H. H.; Cameron, D. G., A Vibrational Study of the Cd2 Stretching Bands of Selectively Deuterated Palmitic and Stearic Acids. *Chemistry and Physics of Lipids* **1982**, *31*, 97.
49. Wang, H.-F.; Gan, W.; Lu, R.; Rao, Y.; Wu, B.-H., Quantitative Spectral and Orientational Analysis in Surface Sum Frequency Generation Vibrational Spectroscopy (Sfg-Vs). *International Reviews in Physical Chemistry* **2005**, *24*, 191-256.
50. Bell, G. R.; Bain, C. D.; Ward, R. N., Sum-Frequency Vibrational Spectroscopy of Soluble Surfactants at the Air/Water Interface. *J. Chem. Soc., Faraday Trans.* **1996**, *92*, 515-23.

51. Guyot-Sionnest, P.; Hunt, J. H.; Shen, Y. R., Sum-Frequency Vibrational Spectroscopy of a Langmuir Film: Study of Molecular Orientation of a Two-Dimensional System. *Phys. Rev. Lett.* **1987**, *59*, 1597-600.
52. Du, Q.; Superfine, R.; Freysz, E.; Shen, Y. R., Vibrational Spectroscopy of Water at the Vapor/Water Interface. *Phys. Rev. Lett.* **1993**, *70*, 2313-16.
53. Kumpulainen, A. J.; Persson, C. M.; Eriksson, J. C.; Tyrode, E. C.; Johnson, C. M., Soluble Monolayers of N-Decyl Glucopyranoside and N-Decyl Maltopyranoside. Phase Changes in the Gaseous to the Liquid-Expanded Range. *Langmuir* **2005**, *21*, 305-315.
54. Du, Q.; Freysz, E.; Shen, Y. R., Surface Vibrational Spectroscopic Studies of Hydrogen Bonding and Hydrophobicity. *Science* **1994**, *264*, 826-8.
55. Björneholm, O., et al., Water at Interfaces. *Chem. Rev.* **2016**.
56. Gonella, G.; Lütgebaucks, C.; de Beer, A. G. F.; Roke, S., Second Harmonic and Sum-Frequency Generation from Aqueous Interfaces Is Modulated by Interference. *J. Phys. Chem. C* **2016**, *120*, 9165-9173.
57. Hore, D. K.; Tyrode, E., Probing Charged Aqueous Interfaces near Critical Angles: Effect of Varying Coherence Length. *J. Phys. Chem. C* **2019**.
58. Ong, S.; Zhao, X.; Eisenthal, K. B., Polarization of Water Molecules at a Charged Interface: Second-Harmonic Studies of the Silica/Water Interface. *Chem. Phys. Lett.* **1992**, *191*, 327-35.
59. Bazant, M. Z.; Kilic, M. S.; Storey, B. D.; Ajdari, A., Towards an Understanding of Induced-Charge Electrokinetics at Large Applied Voltages in Concentrated Solutions. *Advances in Colloid and Interface Science* **2009**, *152*, 48-88.
60. Nightingale, E. R., Phenomenological Theory of Ion Solvation. Effective Radii of Hydrated Ions. *The Journal of Physical Chemistry* **1959**, *63*, 1381-1387.
61. Marcus, Y., Effect of Ions on the Structure of Water: Structure Making and Breaking. *Chem. Rev.* **2009**, *109*, 1346-1370.
62. Brown, M. A.; Abbas, Z.; Kleibert, A.; Green, R. G.; Goel, A.; May, S.; Squires, T. M., Determination of Surface Potential and Electrical Double-Layer Structure at the Aqueous Electrolyte-Nanoparticle Interface. *Phys. Rev. X* **2016**, *6*, 011007.
63. Ben-Yaakov, D.; Andelman, D.; Podgornik, R.; Harries, D., Ion-Specific Hydration Effects: Extending the Poisson-Boltzmann Theory. *Curr. Opin. Colloid Interface Sci.* **2011**, *16*, 542-550.
64. Ben-Yaakov, D.; Andelman, D.; Podgornik, R., Dielectric Decrement as a Source of Ion-Specific Effects. *J. Chem. Phys.* **2011**, *134*, 074705.
65. Ninham, B. W.; Yaminsky, V., Ion Binding and Ion Specificity: The Hoffmeister Effect, Onsager and Lifshitz Theories. *Langmuir* **1997**, *13*, 2097-2108.
66. Parsons, D. F.; Bostrom, M.; Nostro, P. L.; Ninham, B. W., Hofmeister Effects: Interplay of Hydration, Nonelectrostatic Potentials, and Ion Size. *Phys. Chem. Chem. Phys* **2011**, *13*, 12352.
67. Travesset, A.; Vaknin, D., Bjerrum Pairing Correlations at Charged Interfaces. *Europhys. Lett.* **2006**, *74*, 181-187.
68. Kjellander, R., Ion-Ion Correlations and Effective Charges in Electrolyte and Macroion Systems. *Berichte der Bunsengesellschaft für physikalische Chemie* **1996**, *100*, 894-904.
69. Abrashkin, A.; Andelman, D.; Orland, H., Dipolar Poisson-Boltzmann Equation: Ions and Dipoles Close to Charge Interfaces. *Phys. Rev. Lett.* **2007**, *99*, 077801.
70. Parsons, D. F.; Duignan, T.; Salis, A., Cation Effects on Haemoglobin Aggregation: Balance of Chemisorption against Physisorption of Ions. *Interface Foc.* **2017**, *7*, 20160137.

TOC

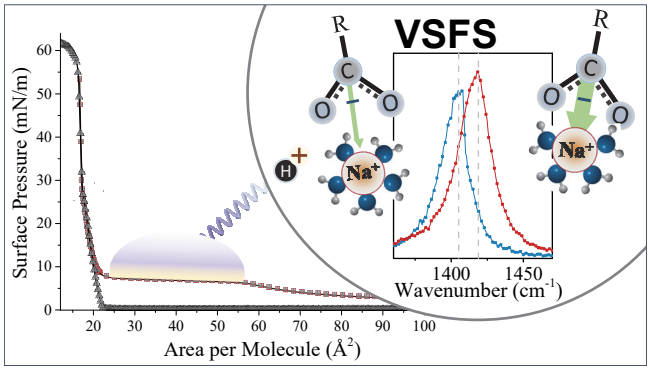
VSFS
Surface Pressure (mN/m)
Area per Molecule (Å²)
Wavenumber (cm⁻¹)
1400
1450
R
C
O
Na⁺
H⁺